Interannual-to-decadal variability of North Atlantic air-sea CO2 fluxes

Stéphane Raynaud, Olivier Aumont, Keith B. Rodgers, Pascal Yiou, James C. Orr

Ocean Science Discussions, 2, 437–472, 2005
www.ocean-science.net/osd/2/437/
SRef-ID: 1812-0822/osd/2005-2-437
European Geosciences Union

Ocean Science Discussions

Papers published in *Ocean Science Discussions* are under open-access review for the journal *Ocean Science*

Interannual-to-decadal variability of North Atlantic air-sea CO_2 fluxes

S. Raynaud[1], O. Aumont[2], K. B. Rodgers[2], P. Yiou[1], and J. C. Orr[1]

[1]Laboratoire des Sciences du Climat et de l'Environnement, CEA, Gif-sur-Yvette, France
[2]Laboratoire d'Océanographie Dynamique et de Climatologie, Paris, France

Received: 11 July 2005 – Accepted: 8 August 2005 – Published: 30 August 2005

Correspondence to: S. Raynaud (stephane.raynaud@cea.fr)

Abstract

The magnitude of the interannual variability of North Atlantic air-sea CO_2 fluxes remains uncertain. Fluxes inferred from atmospheric inversions have large variability, whereas those simulated by ocean models have small variability. Part of the difference is that unlike typical atmospheric inversions, ocean models come with spatial resolution at the sub-basin scale.

Here we explore sub-basin-scale spatiotemporal variability in the North Atlantic in one ocean model in order to better understand why the the North Atlantic basin may well contribute very little to the global variability of air-sea CO_2 flux.

We made two simulations with a biogeochemical model coupled to a global ocean general circulation model (OGCM), which itself was forced by 55-year NCEP reanalysis fields. In the first simulation, atmospheric CO_2 was maintained at the preindustrial level (278 ppmv); in the second simulation, atmospheric CO_2 followed the observed increase. Simulated air-sea CO_2 fluxes and associated variables were analysed with a statistical tool known as multichannel singular spectrum analysis (MSSA).

We found that the subtropical gyre is not the largest contributor to the overall, basin-wide variability, in contrast to previous suggestions. The subpolar gyre and the inter-gyre region (the transition area between subpolar and subtropical gyres) also contribute with multipolar anomalies at multiple frequencies: these tend to cancel one another in terms of the basin-wide air-sea CO_2 flux. We found a strong correlation between the air-sea CO_2 fluxes and the North Atlantic Oscillation (NAO), but only if one takes into account time lags as does MSSA (maximum r=0.64 for lags between 1 and 3 years). The contribution of anthropogenic CO_2 to total variability was negligible at interannual time scales, whereas at the decadal (13-year) time scale, it increased variability by 30%.

OSD

2, 437–472, 2005

1. Introduction

Until recently, atmospheric inversions (Bousquet et al., 2000; Peylin et al., 2004) have assumed that the interannual variability of North Atlantic air-sea CO_2 fluxes was spatially coherent. and that this results in large variability, when integrated arealy. Thus they predict large interannual variability when fluxes are integrated across the basin. Gruber et al. (2002) found these basin-wide fluxes from inverse models were similar to those estimated by extrapolating ocean observations from a subtropical time-series station to the entire North Atlantic basin. In contrast ocean models, which have higher spatial resolution and solve for internal ocean processes from first principles, find only small variability in the North Atlantic. Total simulated variability from ocean models is much larger and that is dominated by the equatorial Pacific. Such small basin-wide variability in the North Atlantic implies that ocean models develop compensating patterns and processes (Le Quéré et al., 2000, 2003a; McKinley et al., 2004b). A recently developed atmospheric inversion approach with much higher horizontal resolution than used previously now indicates small variability of air-sea CO_2 fluxes over the North Atlantic, in much better agreement with ocean models (McKinley et al., 2004b).

In terms of climate variability, interannual-to-decadal changes over the North Atlantic basin are dominated by the North Atlantic Oscillation (NAO) (Hurrell et al., 2003a). The ocean responds to the NAO with a resulting frequency-dependent signature (Visbeck et al., 2003). It has also been suggested that changes in sea ice as well as those within the ocean may have a small feedback on NAO (Czaja et al., 2003; Deser et al., 2000; Lu and Greatbatch, 2002). This complex climate system affects the marine ecosystem, e.g. through changes in circulation and mixed layer depth (Joyce et al., 2000; Marsh, 2000; Le Quéré et al., 2003b) which affects nutrient and light availability and thus export production (Dutkiewicz et al., 2001; Oschlies, 2001). In addition, air-sea CO_2 flux rates depend on NAO in the sense that NAO drives changes in wind, temperature, and ice cover.

Yet with only one relatively long North Atlantic time series station, the Bermuda At-

OSD
2, 437–472, 2005

lantic Time-Series (BATS), our understanding of basin-wide variability of air-sea CO_2 flux is limited. Such a station might be adequate if air-sea fluxes were to act in unison across the basin (Gruber et al., 2002). Such is clearly not the case in ocean models, and even in a new state-of-the-art atmospheric inversion (McKinley et al., 2004a). Furthermore, with only 20 years of data from BATS, we cannot examine decadal oscillations.

Another problem is that, assuming the link between these fluxes and the NAO is partly natural (cf. discussion above), this further complicates disentangling mechanisms and correlations. For example, one cannot ignore possible temporal lags as with EOF analysis. Furthermore, the ocean response to atmospheric forcing differs on interannual and decadal time scales; the same holds for patterns of air-sea CO_2 fluxes.

2. Simulations and analysis tool

2.1. Models

We used the dynamic ocean model known as ORCA2, a generic acronym for OPA (Océan Parallélisé), namely version 8.2 (Madec et al., 1998). ORCA2 is coupled to the dynamic-thermodynamic Louvain-la-Neuve Ice Model (LIM) (Timmermann et al., 2005). ORCA2 has approximately 2° resolution in the extratropics, with meridional resolution increasing to 0.5° at the equator. The ocean model includes 30 vertical levels, with 20 of these in the upper 500 m. The equation of state is calculated using the algorithm of Jackett and McDougall (1995). The bottom boundary layer parameterisation of Beckman and Doscher (1997) was used to represent the flow of deep water over bathymetry. This is the same model configuration as used in previous study of interannual variability (Rodgers et al., 2004) except that here the model also includes a free surface formulated to conserve salt globally (Roullet and Madec, 2000). Lateral mixing is oriented along isopycnal surfaces and includes the mesoscale eddy parameterisation of Gent and McWilliams (1990), except between 10° S and 10° N. Vertical mixing

is achieved using the turbulent kinetic energy (TKE) scheme of Blanke and Delecluse (1993). Modeled surface salinities are restored to climatological values of Boyer et al. (1998). However, the global integral of the restored surface freshwater flux does not necessarily conserve global ocean volume. Hence we computed the globally averaged change in sea level height at the end of each year, and during the following year, we applied a corrective (negative) flux (uniform in space and time) over the surface ocean. Thus the model conserves ocean volume over our multi-decadal integrations.

The biogeochemical model known as the Pelagic Interaction Scheme for Carbon and Ecosystem Studies (PISCES) currently has twenty-four compartments (Bopp et al., 2003, Aumont and Bopp, 2005[1]; Bopp et al., 2005[2]). Five of these are nutrients that limit phytoplankton growth: nitrate plus ammonium, phosphate, silicate, and iron. Yet phosphate and nitrate+ammonium are not independent. They are linked by constant Redfield ratios. However, the nitrogen pool is also affected by nitrogen fixation and denitrification. Setting these two processes to zero would mean that the distribution of nitrogen and phosphate would differ only by the constant Redfield ratio, given equivalent global sizes for these two pools. PISCES also includes four living compartments. These functional groups include two phytoplankton size classes (nanophytoplankton and diatoms) and two zooplankton size classes (microzooplankton and mesozooplankton). For phytoplankton, prognostic variables include total biomass, iron, chlorophyll, and silicon contents. Thus the model predicts the Fe/C, Chl/C, and Si/C ratios of both phytoplankton groups. For zooplankton, only the total biomass is modeled explicitly. For all species, their internal O_2:C:N:P ratios are constant. The bacterial pool is not included.

Additionally, PISCES includes three non-living compartments: small sinking parti-

[1] Aumont, O. and Bopp, L.: Globalizing results from ocean in situ iron fertilization studies, Nature, submitted, 2005.

[2] Bopp, L., Aumont, O., Alvain, S., P.Cadule, and Gehlen, M.: Response of diatoms distribution to global warming and potential implications – A global model study, Geophys. Res. Lett., submitted, 2005.

cles, big sinking particles, and semi-labile dissolved organic matter. As with the living compartments, constant C:N:P ratios are imposed;they are not modeled explicitly. Conversely, the iron, silicon, and calcite pools of the particles are modeled explicitly and their ratios are allowed to vary. Calcite and biogenic silica are assumed to have the same sinking speed as do big particles. In PISCES, all the non-living compartments aggregate as a function of turbulence and differential settling. In addition to these ecosystem variables, PISCES also simulates dissolved inorganic carbon (DIC), total alkalinity and dissolved O_2. A complete description of the PISCES model is accessible from its website (http://www.lodyc.jussieu.fr/~aumont).

2.2. Simulations

To model interannual variability, we forced our simulations with interannually varying reanalysis fields from the National Center of Environmental Prediction (NCEP) during 1948–2002 (55 years). The PISCES model was first integrated offline for 5000 years using climatological circulation fields, with atmospheric CO_2 held at 278 ppmv. At this time, the model tracer fields had reached a near-steady state, which we arbitrarily defined as being the preindustrial state (year 1838). From 1838, it requires three consecutive 55-year cycles to reach the final year of our simulation, 2002. Thus for this industrial era (1838 onward), a "historical" simulation was made where the model's atmosphere was forced to follow observed annual mean CO_2, as provided by the OCMIP-3/NOCES project. Secondly, we made a "control" simulation where atmospheric CO_2 was maintained at 278 ppmv. From the start of 1838 until the end of 1947 (the first two 55-year cycles), we used climatological circulation fields, offline. We present results from both simulations from the 3rd 55-year cycle (1948 to 2002) where PISCES was integrated in the online model.

The daily-mean wind-stress fields for the NCEP reanalysis (Kalnay et al., 1996) are used to force the ocean model at the surface. The wind speeds used for heat and evaporative fluxes in the bulk formulas as well as for gas exchange are calculated from the daily zonal and meridional components of the 10-m winds.

2.3. Analysis

To analyse complex spatiotemporal structures and potential correlations between fields, we used Multi-channel Singular Spectrum Analysis (MSSA, Plaut and Vautard, 1994). Previously MSSA has been used to extract time-dependent structures over the North Atlantic (Moron et al., 1998; Avoird, 2002; Da Costa and de Verdière, 2002). MSSA naturally accounts for lags, intermittency of oscillations, and frequency dependencies such as those that characterise the ocean and atmospheric variability in the North Atlantic.

Here we have used MSSA to extract the natural modes of variability that have a signature in space and time. We decomposed the full signal into oscillations, nonlinear trends, and white noise. Each oscillation represents a possible mode of variability, having a specific period, space-time signature, and intermittency. MSSA goes beyond the classical decomposition with Empirical Orthogonal Functions (EOF) because it is able to extract anomalies that propagate in space and time. Another advantage of MSSA is that it has no a priori assumption about spatio-temporal structure.

To analyze interannual-to-decadal variability of air-sea CO_2 flux we treated all variables of interest simultaneously. Thus we avoid using a simple NAO index that may not be representative of the NAO (Jones et al., 2003), much less total variability over the North Atlantic. In climate studies, it has been shown that the two dominant driving variables in terms of what causes variability at the air-sea interface are the sea surface temperature (SST) and sea level pressure (SLP) (Czaja et al., 2003). The SLP affects both wind stress and wind speed, terms that are used in the model's formulations for exchange of momentum and gases across the air-sea interface. Thus we used SST, wind stress modulus, and the CO_2 flux as the three primary variables in our MSSA analysis. Prior to making the MSSA analysis, model output was first preprocessed by taking 6-month unweighted running means, then removing the annual cycle and the overall linear trend. Then we used EOF analysis (also called Principal Component Analysis) to reduce the number of degrees of freedom from the total number of ocean

surface grid points to only 15. As a final step in preprocessing we normalized all variables independently because they have different units. The dominant climate variables (SST and wind stress), known as the active variables, were given a weight of 1; all others, denoted as passive variables, were given weights of 0.1. Once the MSSA analysis is complete, one is left with statistical modes that can be grouped or studied separately. Oscillations are identified as pairs of modes having similar characteristics. MSSA assumes that the variability is not highly nonlinear. We demonstrate in Sects. 3.6 and 3.7 that nonlinearities here are typically small, meaning our linear decomposition is generally accurate. Our sensitivity tests with other weights and temporal windows for the MSSA analysis do not alter our conclusions.

3. Results

3.1. Annual cycle

As a prerequisite to simulating interannual variability, a model should first be able to simulate a reasonable annual cycle. Fig. 1 compares results from our historical simulation to to data-based monthly maps of ΔpCO_2 (Takahashi et al., 2002) in the North Atlantic.

In winter, the whole basin acts as a sink for the atmospheric CO_2.

Lowest values are found at the southern and north western boundaries. In summer, the southern part of the basin becomes a source. However, this comparison reveals deficiencies particularly where the Gulf-Stream is observed to be most intense South-East of Newfoundland. As with other coarse-resolution models, the Gulf Stream is too weak and continues flowing northward when it should break off to the east. These problems contribute to model errors. During winter, the simulated air-to-sea flux is too large in the west; during summer it is redistributed along the American coast, thereby affecting the amplitude.

3.2. Variability at the BATS station

The only time series station available to evaluate interannual variability in the North Atlantic is BATS. Figure 2 reveals that the amplitude of modeled variability is underestimated except during the late 1990's; however, the phasing is reasonable. Other models show a somewhat higher amplitude of the variability, but generally similar phasing.

Additionally, coarse resolution models do not simulate mesoscale eddies by definition, and such eddies may contribute to interannual variability (Bates, 2001).

To reveal the extent to which the magnitude of variations at BATS may represent those across the North Atlantic, (Fig. 3 shows the standard deviation of the simulated monthly anomalies (relative to the climatological monthly mean) of the air-sea CO_2 flux. Standard deviations are much lower in the subtropics, where BATS is located. (Fig. 3).

3.3. Relationship between the NAO and the air-sea CO_2 flux

In the North Atlantic, McKinley et al. (2004b) found a negligible correlation between the NAO and the first principal component of the air-sea CO_2 flux and the NAO index. However, their analysis neglected lags in the response of air-sea CO_2 fluxes to the NAO. In contrast, we computed lag correlations between the NAO and the area-integrated air-sea CO_2 flux in the subtropical gyre as well as in the intergyre region (Fig. 4).

A significant correlations was found at zero lag in the subtropical gyre (r=−0.56).

However, in the intergyre region, the maximum correlation is found with a lag of 2.5 years (r=0.43). In the subpolar gyre, the correlation is r=−0.31 near zero lag. Spatial inhomogeneity of these lags may result in compensations at zero lag. It will be shown that simulated CO_2 fluxes lag the climate forcing by up to 3 years.

Figure 5 shows that the area-integrated air-sea CO_2 flux over the subpolar gyre is slightly larger than that over the subtropical gyre. Furthermore, despite the subpolar gyre's smaller areal extent, the standard deviation of its area-integrated variability is 20% larger than that for the subtropical gyre (see also Fig. 3).

As for timing, some major events do occur simultaneously in both gyres, yet such

is far from being a general rule (Fig. 5). Additionally, there is more low frequency variability in the subpolar gyre relative to the subtropical gyre. In summary, our simple analysis so far indicates the importance of taking lags into account and of explicitly resolving both gyres, individually.

To properly describe variability of air-sea CO_2 fluxes in the North Atlantic, we need a method that accounts for correlations between variables having complex spatiotemporal structure. Furthermore, we need to distinguish interannual from decadal variability.

3.4. Spectral properties

With MSSA, we evaluated the total contribution of each of the dominant oscillations of the area-integrated, air-sea CO_2 flux (Fig. 6).

The signal is decomposed into four major modes: (1) a first "interannual" oscillatory mode with a 3.2-year period representing 5.0% of the total variance; (2) a second "interannual" oscillatory mode with a 5–7 year period representing 6.4% of the total variance; (3) a "decadal" mode with a period of around 13 years, which is poorly resolved with just a 55-year time series but which contributes 12.7% to the total variance and is the dominant oscillatory mode; and (4) an "interdecadal" mode (not shown) represented by a single non-oscillatory MSSA mode (nonlinear trend) that contributes 14% to the total variance of air-sea CO_2 flux. These frequencies are typical for NAO spectra Hurrell et al. (2003b). For instance, the decadal mode and 5–7 year interannual mode were reported by Moron et al. (1998). Also, roughly 3- and 7-year frequencies were found for the response of ocean heat transport to the NCEP reanalysis forcing (Gulev et al., 2003).

Figure 7 shows the amplitude of anomalies for SST where its values are maximal and the basin-wide integrated air-sea CO_2 flux, plotted along with the average period of each mode. In both simulations all climate variables, including SST and wind, are identical. Yet our MSSA analysis was performed in combination with the CO_2 flux, which differs between the two simulations. Consequently, the resulting modes of variability could differ even in terms of SST and wind. Such effects are reduced, however,

by our choice to use the 1/10 weighting coefficient for the air-sea CO_2 flux in our MSSA analysis (see Sect. 2.3). Moreover, there are no significant difference between the two curves for SST in Fig. 7, which provides confidence that our analysis method is robust.

The air-sea CO_2 flux differences are also negligible for the two interannual modes. In contrast, the amplitude of the basin-wide integrated air-sea flux of CO_2 decadal variability increases by 30% in the historical simulation relative to that in the control simulation. It appears then that decadal variability of air-sea CO_2 fluxes could continue to increase its dominance over interannual variability as atmospheric CO_2 increases in the future.

3.5. Spatiotemporal description

Here following we consider each mode of variability as an oscillation that is a repeated cycle over the length of the simulation. To provide greater physical meaning to our analysis and improve statistical significance, we chose not to interpret the spatiotemporal structure of the modes at a given time during the simulation. Instead, we made composites cycles, i.e. an averaged cycle for each mode (see Da Costa and Vautard, 1997). Each composite cycle was decomposed into 8 parts (phases) in order to evaluate its spatiotemporal evolution. For example, such an approach is commonly used to compute annual cycles with a 12 phases (monthly) decomposition. Our composites for the decadal mode are shown in Fig. 8 whereas those for the two interannual modes are shown in Figs. 9 and 10.

We provide composite maps only for SST and the air-sea CO_2 flux. Maps of wind stress modulus anomalies are not shown because they add little new, relevant information. We chose to display composite maps at only 2 of the 8 phases (a transitory phase and an extreme phase) because one does not loose information by summarising a sinusoidal cycle over a quarter of its period. We arbitrarily define the extreme phase as that when SST anomalies are highest. That always occurs in the 7th part of the 8-phase cycle. We further define the transitory phase as the advance phase quadrature compared to the extreme phase, i.e. the 5th part of the 8-phase cycle.

OSD
2, 437–472, 2005

All modes for SST show features that are characteristic of the NAO (see Hurrell et al., 2003a, and references therein). Wind stress shows the same features but is not displayed. The dominant pattern for SST anomalies is a north-south dipole, particularly in the extreme phase. This dipole results from variability in the Gulf Stream position. This pattern is associated with a variability of the strong westward winds (not shown) over the subpolar gyre. These winds are closely related to the variations in the NAO index. Although there are differences in this dipole among the three dominant modes, differences concern mainly the transitory phases and do not affect their NAO-like signature. Our 5–7 year interannual mode shown here is similar in structure to the 7.7-year mode of Da Costa and de Verdière (2002).

South of 35° N, air-sea CO_2 flux anomalies generally follow SST anomalies in all modes and phases. Such SST dependence is known for the annual cycle in the subtropical gyre (Takahashi et al., 2002). In this latitude range, CO_2 flux anomalies are of the similar amplitudes at all frequencies. Often anomalies having different signs partly cancel one another between the east and the west (e.g. see Fig. 8d).

North of 35° N, there exists no clear relationship between anomalies of SST and those of the air-sea CO_2 flux. Thus outside of the subtropical gyre, the system is more complex in terms of what drives interannual-to-decadal variability of air-sea CO_2 fluxes. Northern anomalies for the air-sea CO_2 flux are much larger for the decadal mode than for the interannual modes, especially during the extreme phases.

The decadal mode is nearly stationary, with large positive anomalies covering the intergyre region and the eastern subpolar gyre; small anomalies of opposite sign are found near Greenland. North of 40° N, the extreme phases of the two interannual modes have some similarities. They exhibit anomalies of one sign in the central intergyre and near Greenland, with anomalies of opposite sign in the eastern and western subpolar gyre (Figs. 9d and 10d). These anomalies tend to cancel each another. Conversely, for the 5–7 year interannual mode during the transitory phase, anomalies are more homogeneous (Fig. 9). Anomalies in the western portion of the subpolar gyre are larger than those in the eastern subpolar gyre and they have the same sign as eastern

subtropical anomalies; these patterns are in sharp contrast with those in the transitory phase of the 3.2-year interannual mode. Thus the 5–7 year interannual mode has air-sea CO_2 flux anomalies, when integrated across the basin, that are larger during the transitory than during the extreme phases. Hence this variability is not in phase with the SST and wind stress anomalies.

Complex spatiotemporal patterns means that anomalies in one part of the basin partially cancel those elsewhere. As an illustration, if we were to neglect the differences in the sign of anomalies, the area integrated basin-wide air-sea CO_2 flux would be 2 to 3 times larger in terms of interannual-to-decadal variability. Spatiotemporal complexity also implies lags in the response of the fluxes to climate forcing.

For example, where wind speed anomalies are largest, off the coast of Ireland, we evaluated the corresponding lag for the air-sea flux (Fig. 11).

Summing all three oscillatory modes, the correlation is largest when flux anomalies lag wind speed by 1 to 3 years. At zero lag, the correlation is not significant.

3.6. Inferred processes

The large surface area of the subtropical gyre suggests anomalies there could dominate basin-wide variability of air-sea CO_2 fluxes, if they were not canceled by anomalies elsewhere. However, we have already showed that intergyre and subpolar air-sea CO_2 flux anomalies are substantial contributors and that those are often opposed to subtropical anomalies. We have also shown that the dominant processes that control anomalies in these regions are probably different.

To help distinguish what processes control the air-sea CO_2 flux, we decomposed the basic flux equation into means and anomalies. That is, we write the anomaly of the air-sea CO_2 flux as

$$F'_{CO_2} = (Kg \cdot \Delta pCO_2)' = Kg' \cdot \overline{\Delta pCO_2} + \overline{Kg} \cdot \Delta pCO'_2 ,$$

where Kg is gas exchange coefficient, ΔpCO_2 is the difference between oceanic and atmospheric pCO_2 (partial pressure of CO_2), the prime denotes an anomaly, and the

overbar represents the long-term average (over the length of the simulation). The anomalies of ΔpCO_2 and Kg were extracted by MSSA.

Figure 12 shows zonal integrals of these terms in extreme phases. Additionally, we display these two terms as maps of anomalies for the decadal model, for both transitory and extreme phases (Fig. 13).

Because Kg was not an output variable of the model, we computed it from saved monthly means of temperature, salinity, wind speed, and fractional sea ice cover. Weak linearities lead to errors that affect this 2-term linear decomposition of the air-sea flux (with MSSA). The sum of these two terms is generally similar to the air-sea CO_2 flux estimated directly with MSSA, except north of 55° N. The total flux in these northern latitudes is generally small (Fig. 12), and for the decadal mode it is substantially less than that estimated by the the sum of the 2 linear terms. Furthermore, the complex nature of anomalies in this region means that our decomposition and reconstruction may suffer. However, our conclusions here from the 2-term linear decomposition are consistent with those from comparison of simulations (Sect. 3.7).

The pattern of the Kg' contribution is similar to that for the wind speed anomaly but it is modulated by SST anomalies. Generally there is a dipolar north-south pattern, with larger values to the north. The contribution due to $\Delta pCO_2'$ term is more complex. For the decadal mode, this term dominates during extreme phases with large anomalies having the same sign as those from the Kg' term over latitudes north of 40° N (Fig. 12b). During transitory phases, the $\Delta pCO_2'$ term is considerably weaker than during extreme phases. For the 5–7 year interannual mode (not shown), this term is homogeneous over the whole basin during transitory phases, which explains why the area-integrated air-sea CO_2 flux lags the wind forcing (see Sect. 3.5). The 3.2-year interannual mode (not shown) is generally weak and the two terms tend to cancel one another over the basin.

An other important term is the upwelling of DIC-enriched deep water to the mixed layer. Mixed layer depth variations may provide a good estimator of such vertical exchange.

OSD
2, 437–472, 2005

South of Greenland and throughout much of the subpolar gyre, anomalies of variations in mixed-layer depth for the extreme phase (Fig. 14b) are opposite in sign to those for $\overline{Kg} \cdot \Delta pCO_2'$ (Fig. 13b). Elsewhere, mixing tends to dampen variability of the air-sea CO_2 fluxes.

Deep waters are enriched in nutrients as well as in DIC. Thus variations of the mixed layer depth and greater exchange with deep water means greater nutrient supply to the surface and thus increased particle export of organic matter. Anomalies of variations in large particle export reveal that for the extreme phase (Fig. 14d), these variations reinforce the air-sea CO_2 fluxover most of the North Atlantic, including the subtropical gyre, the intergyre region, and particularly the west subpolar gyre. In contrast to the north variations in particle export appear to go against variations in air-sea CO_2 fluxes; however, these are compensated for by the opposite effect due to variations in mixed layer depth. During the transitory phase, large homogeneous variations in particle export (Fig. 14c) may explain most of the variability of the air-sea flux ((Fig. 8c). This tendency for decadal variability is even more prominent for interannual variability, particularly the longer 5–7 year mode (not shown), which suggests it as one likely cause for the delayed response of the air-sea CO_2 flux to the atmospheric forcing. However, there is an important caveat. These interpretations are qualitative, as are others here based on matching the sign and structure of mapped anomalies. Such provides a first step in using MSSA to analyze complex spatiotemporal variability of physical and biogeochemical variables. Clearly though, there is a need to develop an approach which uses MSSA to quantify the contribution of individual terms to the overall flux.

3.7. Preindustrial versus modern case

As shown in Fig. 7, increased atmospheric CO_2 increases decadal variability of the air-sea CO_2 flux. This increased variability comes from the effect of the increased absolute value of ΔpCO_2 on the $\overline{\Delta pCO_2} \cdot Kg'$ term. The increase in $\overline{\Delta pCO_2}$ between preindustrial (control simulation) and the modern (historical simulation) times, i.e. the anthropogenic

change, is particularly large north of 30° N (Fig. 15a). Thus decadal variability of the historical run is enhanced in the subpolar region and changes sign in the subtropics and intergyre regions (compare Figs. 15b and 8b). Decadal anomalies have become more homogeneous as the area-integrated air-sea CO_2 flux has increased. In the future, as atmospheric CO_2 continues to increase so will $\overline{\Delta pCO_2}$, thereby increasing the contribution of the $\overline{\Delta pCO_2} \cdot Kg'$ term, particularly at decadal timescales.

4. Conclusions

With an OGCM coupled to a biogeochemical model forced by 55 years of NCEP reanalysis winds, we made preindustrial and industrial-era simulations to study the variability of air-sea CO_2 fluxes in the North Atlantic. A basic lag-correlation analysis between the NAO and the air-sea CO_2 flux reveals complex spatiotemporal structure that cannot be resolved with traditional methods, such as EOF analysis. Thus we used MSSA to analyze interannual-to-decadal variability of climate and biogeochemical variables.

An analysis of SST and wind speed shows well known structures and spectral properties that are characteristic of interannual-to-decadal variability over the North Atlantic and of the NAO in particular. Patterns of variability of subtropical air-sea CO_2 fluxes are roughly similar at all frequencies (interannual to decadal), whereas there are substantial differences in pattern between frequencies in the subpolar gyre. Overall, we found that high and low anomalies extend throughout the North Atlantic and partially cancel one another, thereby damping total basin-wide air-sea CO_2 fluxes. There are also delays in the air-sea CO_2 flux relative to climate forcing, with maximum correlation when the flux lags the climate forcing by 1 and 3 years. The 1-year lag may be due to 1-year equilibration time required for perturbations in atmospheric CO_2 to mix throughout the mixed layer (Broecker and Peng, 1974). As shown with qualitative pattern matching, longer lags of up to 3 years may be caused by export production and its links with circulation-driven control factors. Lags on this timescale have been docu-

mented previously in regard to interior ocean dynamics (Hakkinen, 1999; Gulev et al., 2003).

A linear decomposition of the basic air-sea CO_2 flux equation reveals that the variability of Kg and ΔpCO_2 are often similar in intensity and tend to cancel one another. At interannual timescales, the $\overline{Kg} \cdot \Delta pCO_2'$ term is partly responsible for the lag between the climate forcing and the air-sea CO_2 flux. At decadal timescales, the $Kg' \cdot \overline{\Delta pCO_2}$ term plays an important role with large anomalies in the North that partly coincide with those of $\overline{Kg} \cdot \Delta pCO_2'$. The resulting effect becomes obvious by comparing simulations with preindustrial and modern levels of CO_2. Increase in atmospheric CO_2 have enhanced decadal variability. This "geochemical" enhancement of variability is distinct from changes in variability that will be due to future changes in climate.

Others have shown that mesoscale dynamics play an important role southeast of Newfoundland, where eddies affect DIC content as well as other biogeochemical properties (McGillicuddy Jr et al., 1999; Bates, 2001). Certainly, our coarse-resolution model does not explicitly simulate mesoscale eddies in this region. Higher horizontal resolution may well improve model deficiencies in the simulated annual cycle in the air-sea CO_2 flux adjacent to North America in the subtropical gyre and intergyre region. Likewise, higher resolution could alter the large simulated decadal anomalies in this region.

In the future, it would be useful to incorporate the MSSA analysis within the framework of online simulations in order to quantitatively determine the contributions of individual terms to the air-sea CO_2 flux as well as the DIC and alkalinity equations integrated over the mixed layer.

Acknowledgements. We thank G. Madec for discussions. This study was supported by the European Union 5th Framework NOCES project (Contract No. EVK2-CT-2001-00134). Computations where performed at the French CNRS (IDRIS) and CEA (CCRT) supercomputing centers.

References

Avoird, E. v. d.: Low-frequency variability in the coupled ocean-atmosphere system at midlatitudes, Ph.D. thesis, Utrecht Univ., 112 pp., 2002. 443

Bates, N.: Interannual variability of oceanic CO_2 and biogeochemical properties in the Western North Atlantic subtropical gyre, Deep-Sea Research II, 48, 1507–1528, 2001. 445, 453

Beckman, A. and Doscher, R.: A method for improved representation of dense water spreading over topography in geopotential-coordinate models, J. Phys. Oceanogr., 27, 581–591, 1997. 440

Blanke, B. and Delecluse, P.: Low frequency variability of the tropical Atlantic ocean simulated by a general circulation model with two different mixed layer physics, J. Phys. Oceanogr., 23, 1363–1388, 1993. 441

Bopp, L., Kohfeld, K. E., Quéré, C. L., and Aumont, O.: Dust impact on marine biota and atmospheric pCO_2 during glacial periods, Paleoceanogr., 1046, doi:10.1029/2002PA000810, 2003. 441

Bousquet, P., Peylin, P., Ciais, P., Le Quéré, C., Friedlingstein, P., and Tans, P.: Regional changes in carbon dioxide fluxes of land and oceans since 1980, Science, 290, 1342–1346, 2000. 439

Boyer, T. P., Levitus, S., Antonov, J. I., Conkright, M. E., O'Brien, T. D., and Stephens, C.: World Ocean Atlas 1998, NOAA Atlas NESDIS 30, 4, 166 pp., 1998. 441

Broecker, W. S. and Peng, T. H.: Gas exchange rates between air and sea, Tellus, 26, 21, 1974. 452

Czaja, A., Robertson, A. W., and Huck, T.: The role of the Ocean-Atmosphere Coupling Affecting the North Atlantic Variability, in: The North Atlantic Oscillation, edited by: Hurrell, J., Kushnir, Y., Ottersen, G., and Visbeck, M., Geophysical Monograph Series, AGU, 134, 147–172, 2003. 439, 443

Da Costa, E. and de Verdière, A. C.: The 7.7-year North Atlantic Oscillation, Quart. J. Roy. Meteor. Soc., 128, 797–818, 2002. 443, 448

Da Costa, E. and Vautard, R.: A qualitative realistic low-order model of the extratropical low-frequency variability built from long record of potential vorticity, J. Atmos. Sci., 54, 1064–108, 1997. 447

Deser, C., Walsh, J. E., and Timlin, M. S.: Arctic Sea Ice Variability in the Context of Recent Atmospheric Circulation Trends, J. Clim., 13, 617–633, 2000. 439

Dutkiewicz, S., Follows, M., Marshall, J., and Gregg, W. W.: Interannual variability of phytoplankton abundances in the North Atlantic, Deep Sea Res., 48, 2323–2344, 2001. 439
Gent, P. R. and McWilliams, J. C.: Isopycnal mixing in ocean circulation models, J. Phys. Oceanogr., 20, 150–155, 1990. 440
Gruber, N., Bates, N., and Keeling, C. D.: Interannual variability in the North Atlantic carbon sink, Science, 298, 2374–2378, 2002. 439, 440
Gulev, S. K., Barnier, B., Knochel, H., Molines, J.-M., and Cottet, M.: Water mass transformation in the North Atlantic and its impact on the meridional circulation: Insights from an ocean model forced by NCEP-NCAR reanalysis surface fluxes, J. Clim., 16, 3085–3110, 2003. 446, 453
Hakkinen, S.: Variability in the simulated meridional heat transport in the North Atlantic for the period 1951–1993, J. Geophys. Res., 104, 10 991–11 007, 1999. 453
Hurrell, J., Kushnir, Y., Ottersen, G., and Visbeck, M., eds.: The North Atlantic Oscillation: Climate Significance and Environmental Impact, Geophysical Monograph Series, AGU, 134, 2003a. 439, 448
Hurrell, J., Kushnir, Y., Ottersen, G., and Visbeck, M.: An Overview of the North Atlantic Oscillation, in: The North Atlantic Oscillation, edited by: Hurrell, J., Kushnir, Y., Ottersen, G., and Visbeck, M., Geophysical Monograph Series, AGU, 134, 1–36, 2003b. 446
Jackett, D. R. and McDougall, T. J.: Minimal adjustment of hydrographic data to achieve static stability, J. Atmos. Oceanic Technol., 12, 381–389, 1995. 440
Jones, P. D., Osborn, T. J., and Briffa, K. R.: Pressure-Based Measures of the North Atlantic Oscillation (NAO): A Comparison an Assessment of Changes in the Strength of the NAO and in Its Influence on Surface Climate Parameters, in: The North Atlantic Oscillation, edited by: Hurrell, J., Kushnir, Y., Ottersen, G., and Visbeck, M., Geophysical Monograph Series, AGU, 134, 51–62, 2003. 443
Joyce, T. M., Deser, C., and Spall, M. A.: The Relation between Decadal Variability of Subtropical Mode Water and the North Atlantic Oscillation, J. Clim., 13, 2550–2569, 2000. 439
Kalnay, E., Kanamitsu, M., Kistler, R., Collins, W., Deaven, D., Iredell, L. G. M., Saha, S., White, G., Woollen, J., Zhu, Y., Leetmaa, A., Reynolds, R., Chelliah, M., Ebisuzaki, W., W.Higgins, Janowiak, J., Mo, K. C., Ropelewski, C., Wang, J., Jenne, R., and Joseph, D.: The NCEP/NCAR 40-Year Reanalysis Project, Bull. Am. Meteorol. Soc., 77, 437–471, 1996. 442
Le Quéré, C., Orr, J. C., Monfray, P., Aumont, O., and Madec, G.: Interannual variability of the

oceanic sink of CO_2 from 1979 through 1997, Global Biogeochem. Cycles, 14, 1247–1266, 2000. 439
Le Quéré, C., Aumont, O., Bopp, L., Bousquet, P., Ciais, P., Francey, R., Heimann, M., Keeling, R., Kheshgi, H., Peylin, P., Piper, S., and Rayner, I. P.: Two decades of ocean CO_2 sink and variability, Tellus, 55, 649–656, 2003a. 439
Le Quéré, C., Aumont, O., Monfray, P., and Orr, J.: Propagation of climatic events on ocean stratification, marine biology, and CO_2: Case studies over the 1979-1999 period, J. Geophys. Res., C12, 2003b. 439, 459
Lu, J. and Greatbatch, R. J.: The changing relationship between the NAO and northern hemisphere climate variability, Geophys. Res. Lett., 29, 2002. 439
Madec, G., Delecluse, P., Imbard, M., , and Levy, C.: OPA version 8.1 Ocean General Circulation Model Reference Manual, Note du pôle de modélisation, 11, pp. 91, 1998. 440
Marsh, R.: Recent variability of the North Atlantic thermohaline circulation inferred from surface heat and freshwater fluxes, J. Clim., 13, 3239–3260, 2000. 439
McGillicuddy Jr, D. J., Johnson, R., Siegel, D. A., Michaels, A. F., Bates, N. R., and Knap, A. H.: Mesoscale variations of biogeochemical properties in the Sargasso Sea, J. Geophys. Res., 104, 13 381–13 394, 1999. 453
McKinley, G., Rodenbeck, C., Gloor, M., Houweling, S., and Heimann, M.: Emerging agreement between atmospheric inversions and ocean models, Geophys. Res. Lett., p. in press, 2004a. 440
McKinley, G. A., Follows, M. J., and Marshall, J.: Mechanisms of air-sea CO_2 flux variability in the equatorial Pacific and the North Atlantic, Global Biogeochem. Cycles, 18, GB2011, 2004b. 439, 445, 459
Moron, V., Vautard, R., and Ghil, M.: Trends, decadal and inter-annual variability in global sea surface temperature fields, Clim. Dyn., 14, 545–569, 1998. 443, 446
Oschlies, A.: NAO-induced long-term changes in nutrient supply to the surface waters of the North Atlantic, Geophys. Res. Lett., 28, 1751–1757, 2001. 439
Peylin, P., Bousquet, P., Quéré, C. L., Sitch, S., Friedlingstein, P., McKinley, G., Gruber, N., Rayner, P., and Ciais, P.: Interannual CO_2 fluxes as deduced by inverse modeling of atmospheric CO_2 and by models of the ocean and the land carbon cycle, Global Biogeochem, Cycles, in press, 2004. 439
Plaut, G. and Vautard, R.: Spells of low-frequency oscillations and weather regimes in the northern hemisphere, J. Atmos. Sci., 2, 210–236, 1994. 443

Rodgers, K. B., Aumont, O., Madec, G., Menkes, C., Blanke, B., Monfray, P., Orr, J. C., and Schrag, D. P.: Radiocarbon as a thermocline proxy for the eastern equatorial Pacific, Geophys. Res. Lett., 31, L14314, doi:10.1029/2004GL019764, 2004. 440

Roullet, G. and Madec, G.: Salt conservation, free surface and varying volume: a new formulation for Ocean GCMs, J. Geophys. Res., 105, 23 927–23 942, 2000. 440

Takahashi, T., Sutherland, S. C., Sweeney, C., Poisson, A., Metzl, N., Tilbrook, B., Bates, N., Wanninkhof, R., Feely, R. A., Sabine, C., Olafsson, J., and Nojiri, Y.: Global sea-air CO_2 flux based on climatological surface ocean pCO_2, and seasonal biological and temperature effects, Deep Sea Res., 49, 1601–1622, 2002. 444, 448, 458

Timmermann, R., Goosse, H., Madec, G., Fichefet, T., Ethe, C., and Dulière, V.: On the representation of high latitude processes in the ORCA-LIM global coupled sea ice ocean model, Ocean Modelling, 8, 175–201, 2005. 440

Visbeck, M., Chassignet, E., Curry, R., Delworth, T., Dickson, B., and Krahmann, G.: The ocean's response to North Atlantic Oscillation variability, in: The North Atlantic Oscillation, edited by: Hurrell, J., Kushnir, Y., Ottersen, G., and Visbeck, M., Geophysical Monograph Series, AGU, 134, 113–146, 2003. 439

Wetzel, P., Winguth, A., and Maier-Reimer, E.: Sea-to-air CO_2 flux from 1948 to 2003: A model study, Global Biogeochem. Cycles, 19, GB2005, doi:10.1029/2004GB002 339, 2005. 459

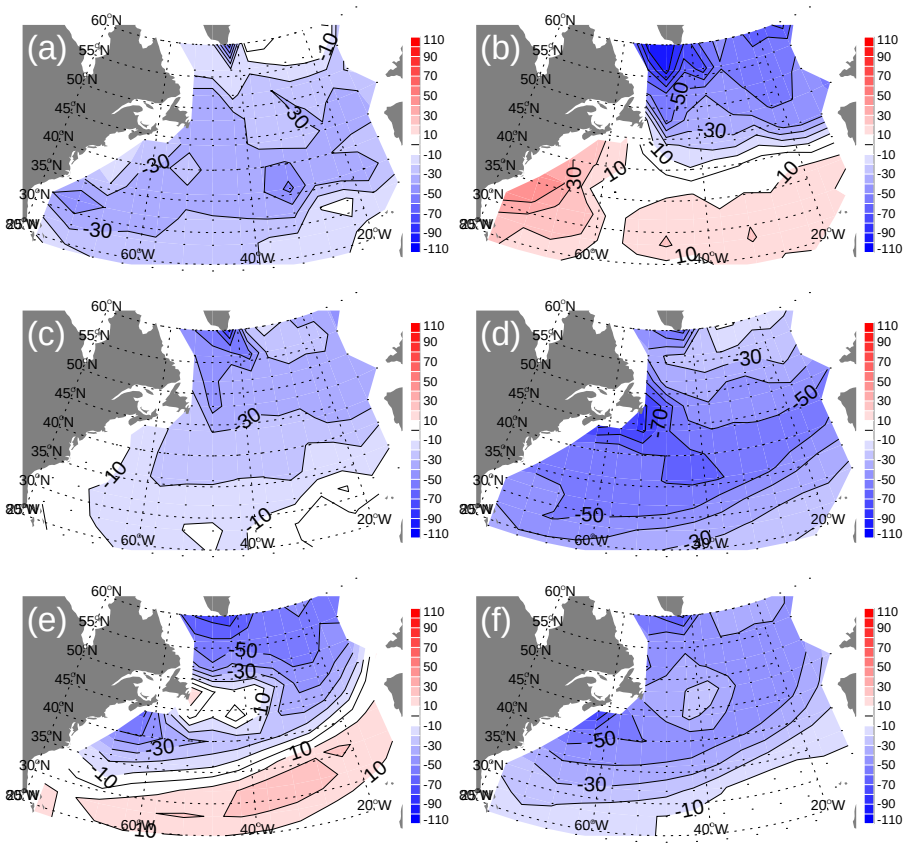

Fig. 1. Annual variations of ΔpCO_2 (Takahashi et al., 2002) in µatm **(a)** winter, **(b)** summer, and **(c)** annual mean observed maps (Takahashi et al., 2002), and the simulated by the model **(d)** winter, **(e)** summer, and **(f)** annual mean computed for the 1990s. Results are mapped using the Lambert equal-area projection.

OSD
2, 437–472, 2005

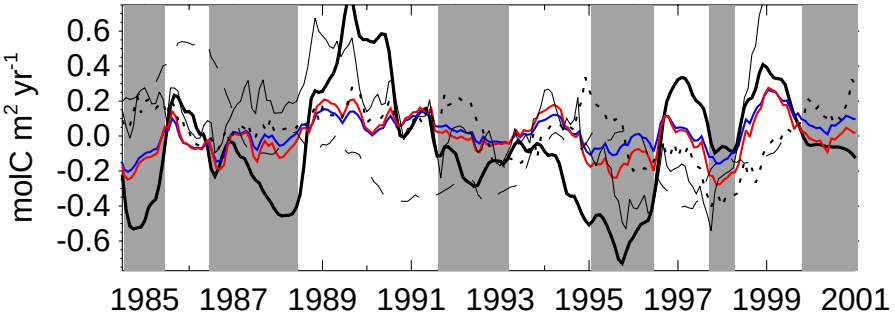

Fig. 2. Times series of the sea-to-air CO_2 flux (molC m^{-2} year^{-1}) for the BATS data (black), the control (blue) and historical (red) simulations as a 2° box average around Bermuda as well as results from three previously published ocean model simulations: Le Quéré et al. (2003b) (dotted), Wetzel et al. (2005) (dashed) and McKinley et al. (2004b) (thin solid). A 12-month running mean was applied to all data. Shaded areas indicate when observed fluxes tend to be from the atmosphere to the ocean.

OSD
2, 437–472, 2005

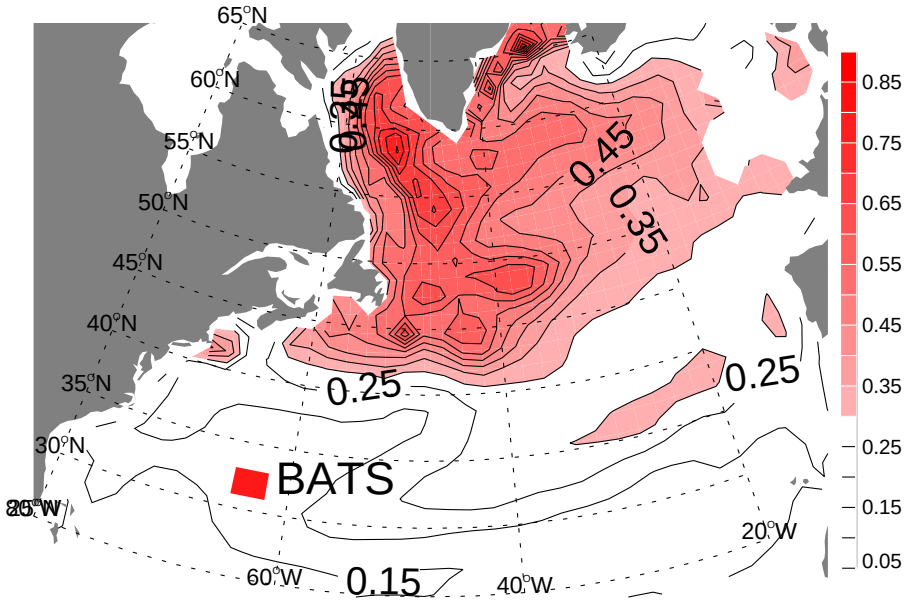

Fig. 3. Standard deviation of the monthly anomalies of the air-sea CO_2 flux (mol C m^{-2} $year^{-1}$) simulated in the historical simulation. A solid square indicates the position of the BATS station.

OSD
2, 437–472, 2005

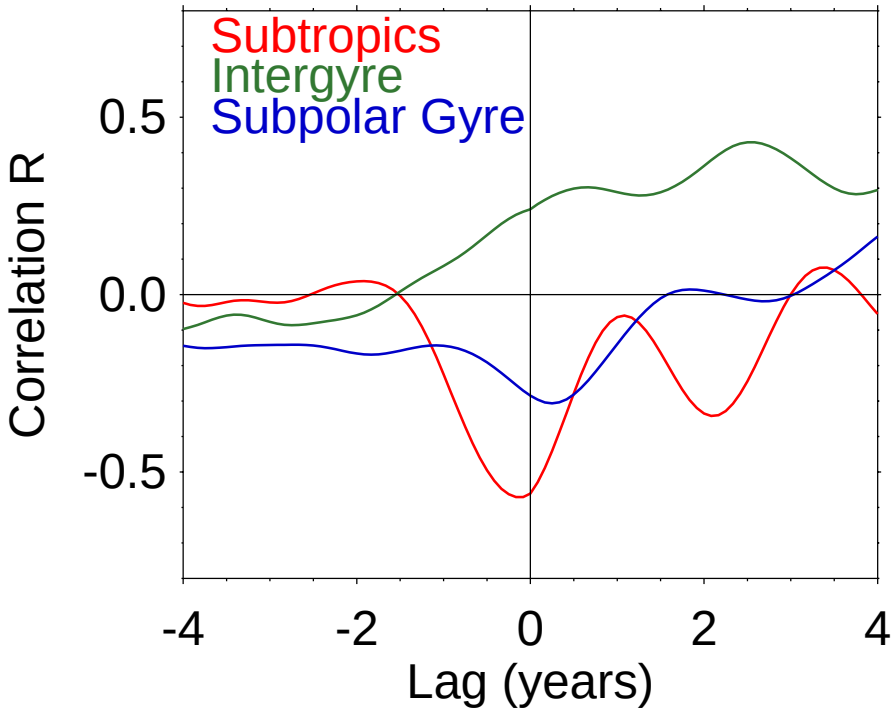

Fig. 4. Lag correlation between the NAO index and the air-sea CO_2 flux in the subtropical region, bounded by 65° W–43° W and 29° N–37° N (red) as well as the intergyre region, bounded by 54° W–21° W and 45° N–52° N (green), and the subpolar bounded by (65° W–43° W, 55° N–60° N) (blue). White noise was removed by MSSA prior to this lag correlation analysis (see Sect. 2.3).

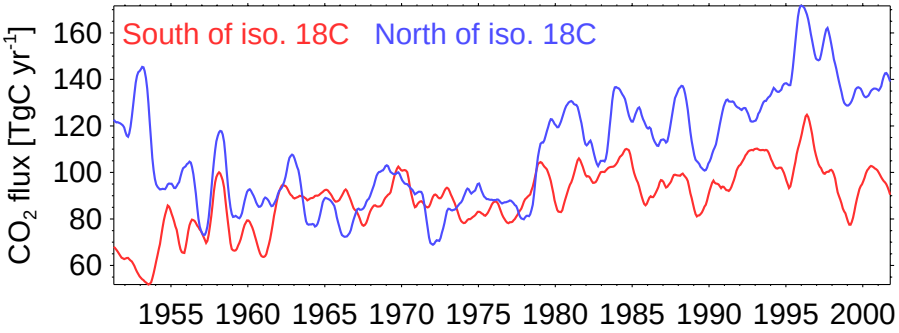

Fig. 5. Times series of the area-integrated CO_2 flux (TgC year^{-1}) over the subtropical gyre (red) and over the intergyre plus subpolar gyre (blue). For simplicity, the limit between the two regions was arbitrarily defined here as the climatological annual mean 18°C surface isotherm.

OSD
2, 437–472, 2005

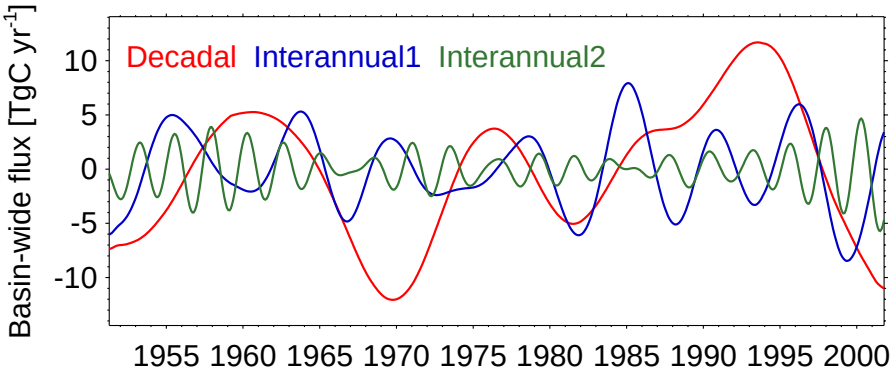

Fig. 6. Anomalies of the basin-wide integrated CO_2 flux (between 20°N and 70°N) in TgC year^{-1} for the ~3.2-year interannual model (green), the 5–7 year interannual mode (blue), and the the 13-year "decadal" mode (red).

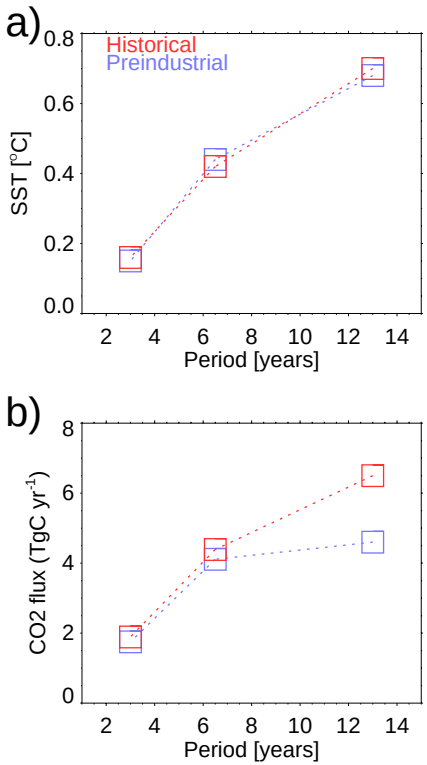

Fig. 7. The amplitude of anomalies for **(a)** maximal SST (°C) and **(b)** basin-wide integrated air-sea CO_2 flux between 20° N and 70° N (TgC year^{-1}) for the control and historical simulations, plotted against the period for each mode.

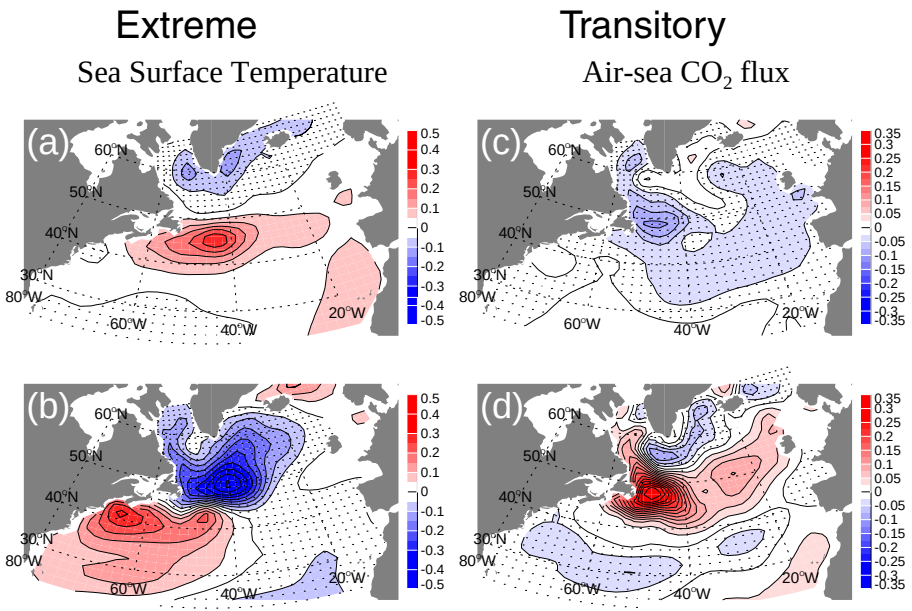

Fig. 8. Anomalies of SST (°C) for the decadal mode during the **(a)** transitory and **(b)** extreme phases of the 8-phase cycles. Corresponding maps are also shown for the **(c)** transitory and **(d)** extreme phases for anomalies of air-sea CO_2 flux (molC m^{-2} $year^{-1}$). Negative values are indicated by dotted areas. A transitory phase occurs a quarter of cycle before an extreme phase.

OSD
2, 437–472, 2005

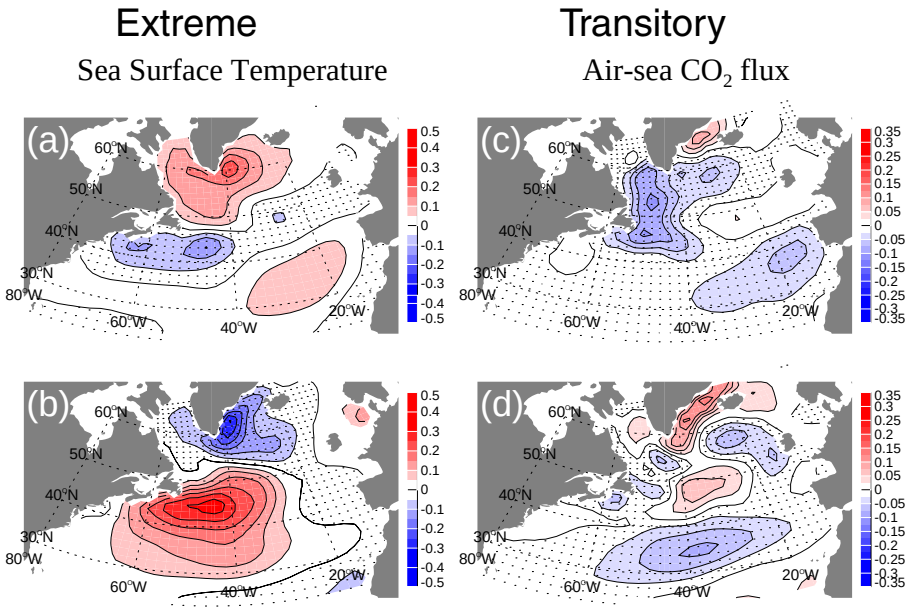

Fig. 9. Anomalies of SST and the air-sea CO_2 flux shown as in Fig. 8, but for the 5–7 year interannual mode.

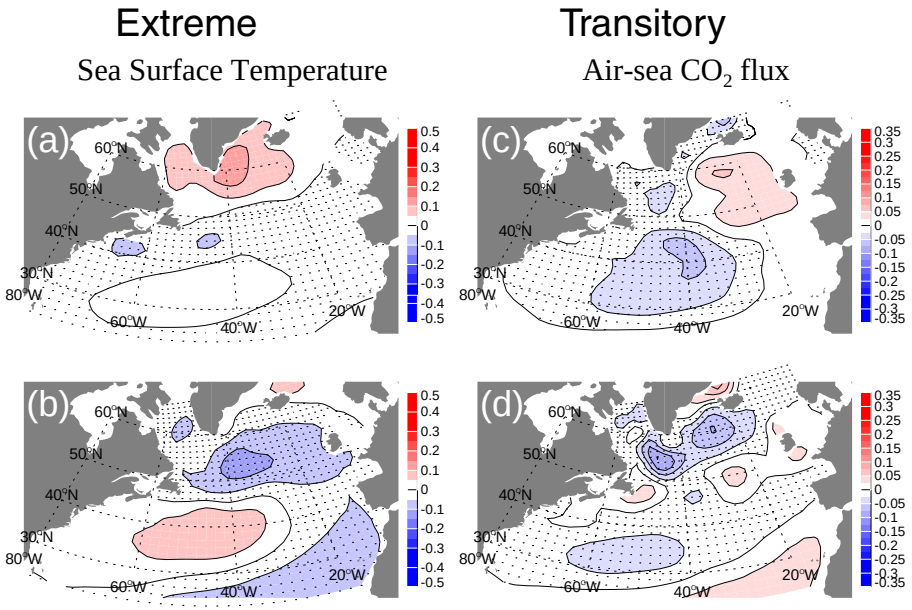

Fig. 10. Anomalies of SST and the air-sea CO_2 fluxshown as in Fig. 8, but for the 3.2-year interannual mode.

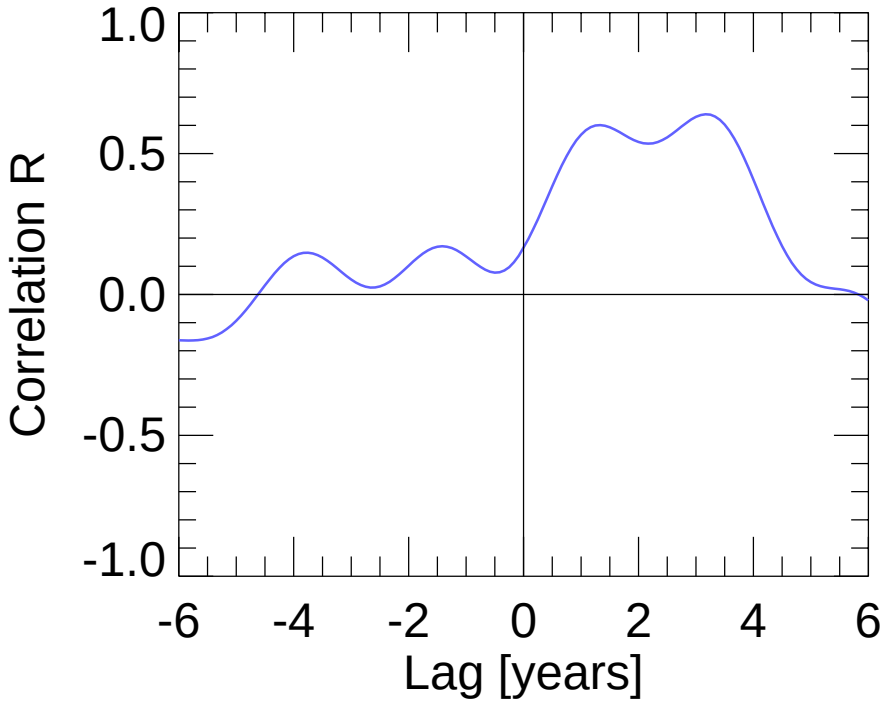

Fig. 11. Lag correlation using the sum of interannual and decadal variability for wind speed off Ireland (where wind anomalies are largest) vs. the air-sea CO_2 flux integrated areally across the basin (20° N to 70° N). Correlation maxima occur when the flux lags wind speed by 1 and 3.1 years.

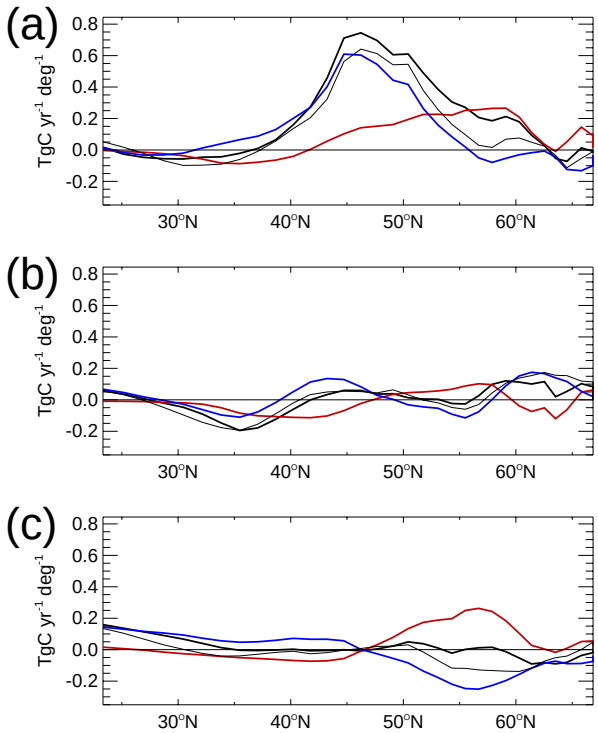

Fig. 12. Zonal integrals in $\mathrm{TgC\,yr^{-1}deg^{-1}}$ for $\overline{Kg'} \cdot \overline{\Delta \mathrm{pCO_2}}$ (red line), $\overline{Kg} \cdot \Delta \mathrm{pCO_2'}$ (blue line), their sum (thick solid line) and the directly estimated air-sea CO_2 flux (thin solid line) for the extreme phases of **(a)** the 13-year decadal mode, **(b)** the 5–7 year interannual mode, and **(c)** the 3.2-year interannual mode.

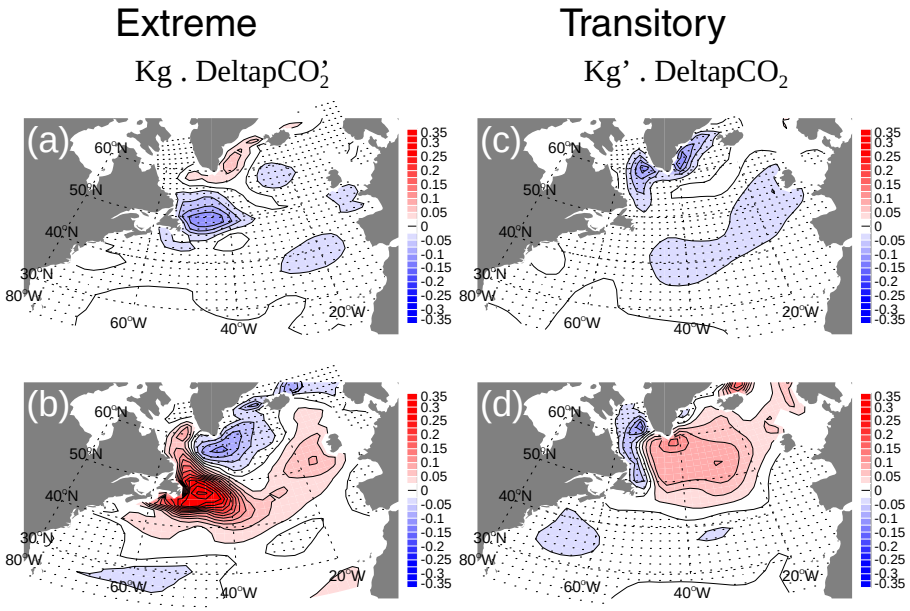

Fig. 13. Decadal mode anomalies for the **(a)** extreme and **(b)** transitory phases of the $\overline{Kg} \cdot \Delta pCO_2'$ term as well as the **(c)** extreme and **(d)** transitory phases of the $Kg' \cdot \overline{\Delta pCO_2}$ term (in mol C year^{-1} m^{-2}). Compare with analogous maps in Fig. 8.

OSD
2, 437–472, 2005

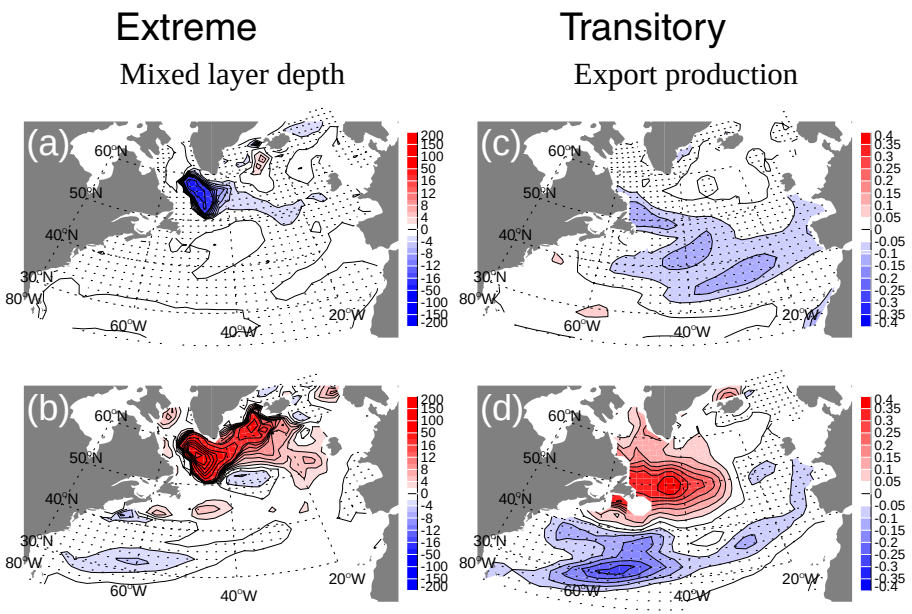

Fig. 14. Decadal mode anomalies of variations in mixed layer depth in m for the **(a)** transitory and **(b)** extreme phases as well as anomalies of export production in mol C m^{-2} $year^{-1}$ for the **(c)** transitory and **(d)** extreme phases.

OSD
2, 437–472, 2005

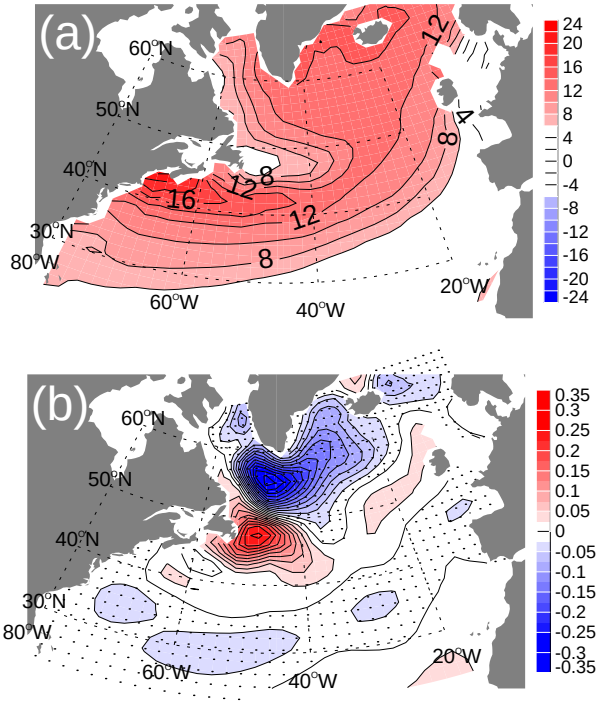

Fig. 15. **(a)** Historical minus preindustrial $\overline{\Delta pCO_2}$ (ppm) and **(b)** decadal variability for the extreme phase of the air-sea CO_2 flux as Fig. 8b but for the control (preindustrial) simulation (mol C m^{-2} $year^{-1}$).

OSD
2, 437–472, 2005